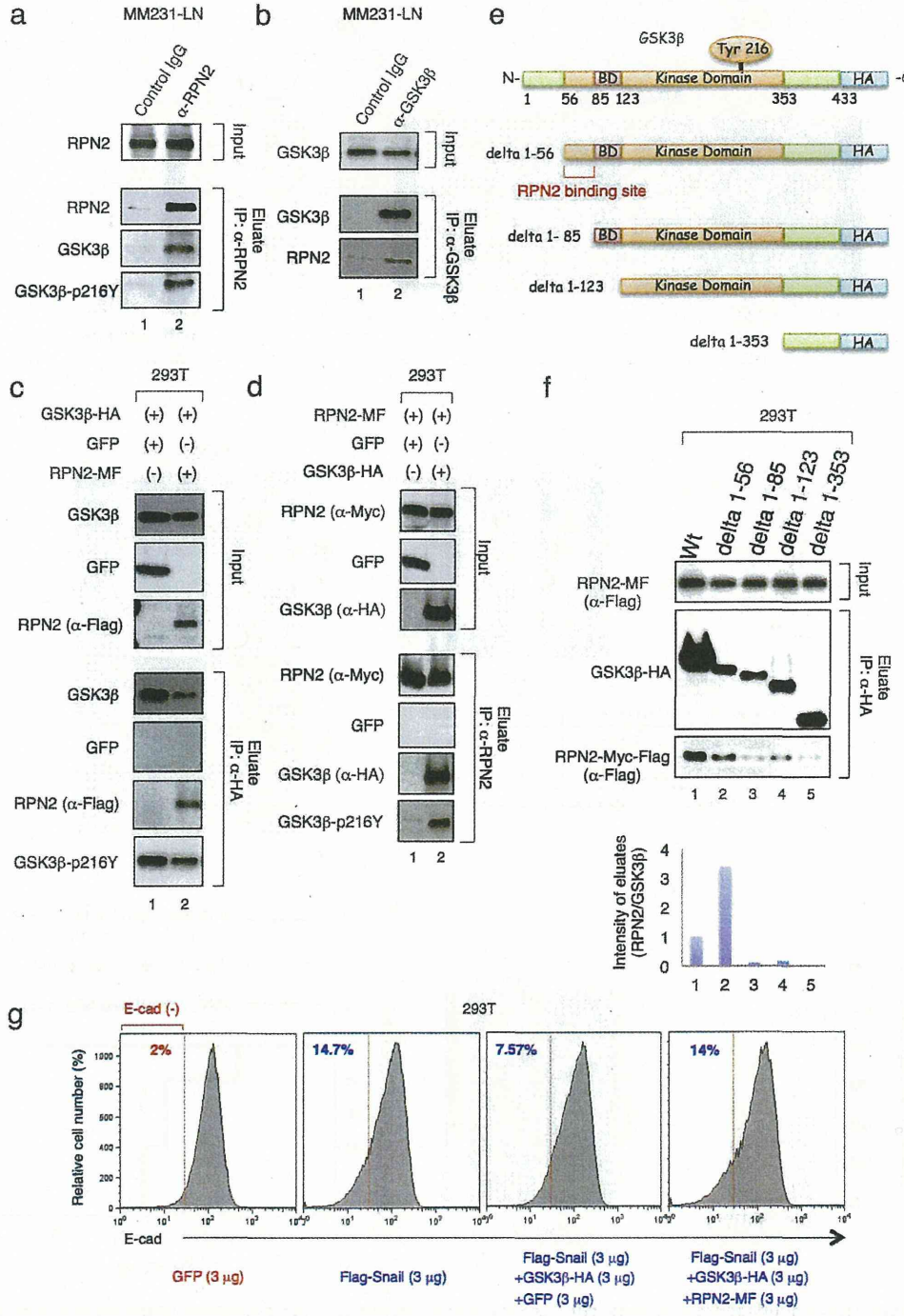

Figure 4 | RPN2 antagonizes GSK3βfunction via physical interaction. (a) and (b) RPN2 associated with GSK3β in MM231-LN cells. In the left panel, cell lysates were subjected to co-immunoprecipitation with an anti-RPN2 antibody and subjected to western blotting with anti-RPN2 (top), anti-GSK3β (middle) or anti-Phospho-GSK3β (Tyr216) antibodies (bottom). In the right panel, cell lysates were subjected to co-immunoprecipitation with an anti-GSK3β antibody and subjected to western blotting with anti-GSK3β (top and middle) and anti-RPN2 antibodies (bottom). (c) GSK3β associated with RPN2 in 293T cells. Cell lysates were subjected to co-immunoprecipitation with anti-HA Agarose and western blotting with anti-GSK3β (top), anti-GFP (middle), anti-RPN2 (bottom) or anti-Phospho-GSK3β (Tyr216) antibodies. (d) RPN2 associated with phosphorylated GSK3β in 293T cells. Cell lysates were subjected to co-immunoprecipitation with an anti-RPN2 antibody and western blotting with anti-RPN2 (top), anti-GFP (middle), anti-GSK3β (bottom) or anti-Phospho-GSK3β (Tyr216) antibodies. (e) Schematic representation of GSK3β and its deletion mutants. The binding domain (BD) designates the GSK3β-specific binding sites for its substrates and protein complexes. (f) RPN2-Myc-Flag, GSK3β-HA and the GSK3β deletion mutants were expressed in 293T cells and immunoprecipitated (IP) with an anti-HA antibody. Lysates (input) and immunoprecipitates were immunoblotted to detect co-immunoprecipitated RPN2. (g) Flow cytometry analysis and quantification of the percentage of E-cadherin-negative cells in 293T cells at 48 h after transfection. The amount of plasmid DNA used in each experiment was indicated in the figure. Full-length gels and blots are shown in supplementary figure 13 and 14.

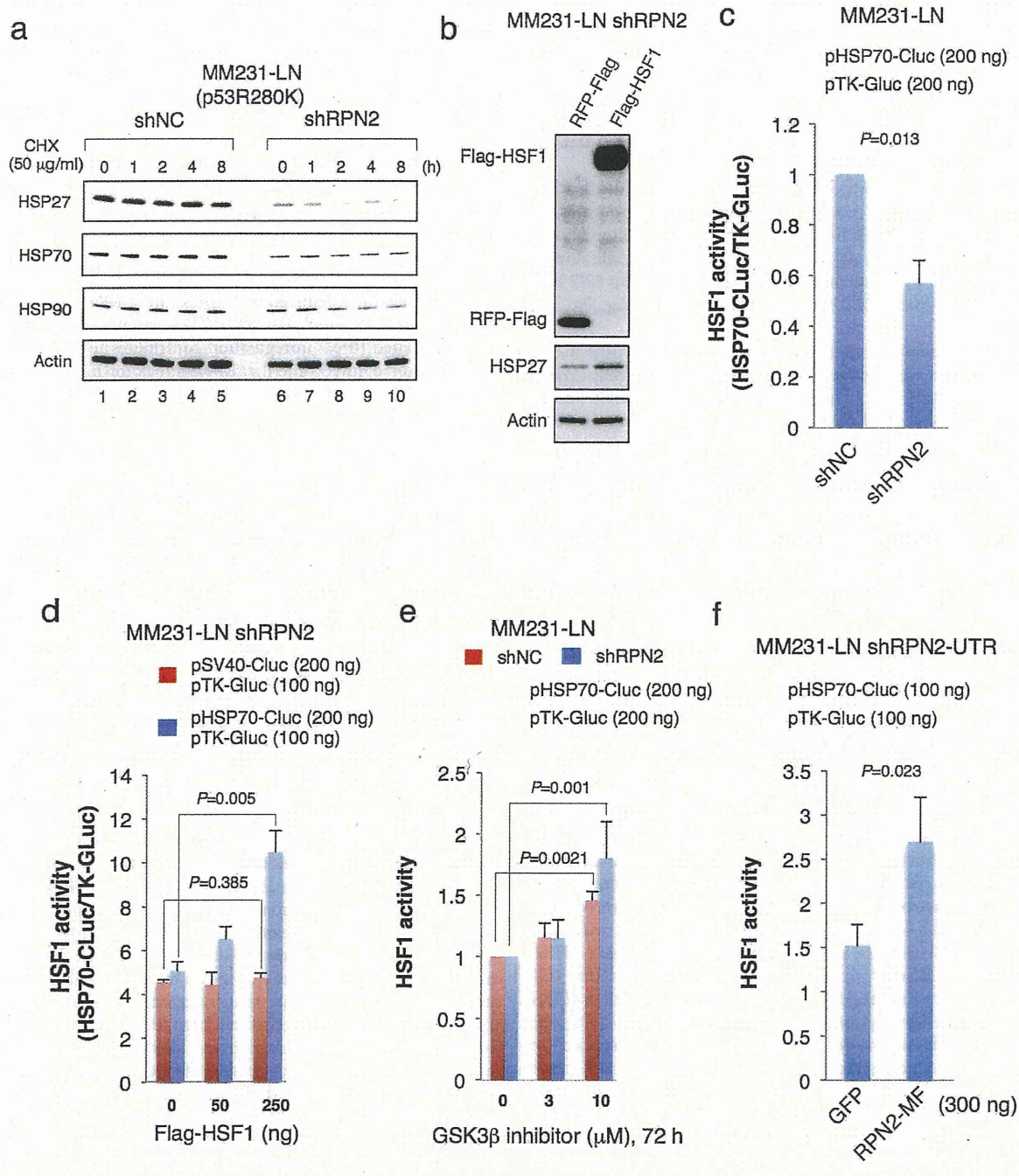

Figure 5 | RPN2 knockdown suppressed the heat shock proteins via GSK3β activation. (a) RPN2 knockdown suppressed the expression of HSP27 and HSP70 and reduced HSP90 protein stability. MM231-LN shNC and MM231-LN shRPN2 cells were treated with cycloheximide (50 μg/ml) for 0–8 h. Cell lysates were subjected to western blotting with anti-HSP27, anti-HSP70, anti-HSP90 and anti-actin antibodies. (b) HSF1 restored the HSP27 expression in MM231-LN shRPN2 cells. After transfection of pFlag-HSF1 into MM231-LN shRPN2 cells, Cell lysates were subjected to western blotting with anti-Flag (top), anti-HSP27 (middle), anti-actin (bottom) antibodies. (c) HSF1 transcriptional activity in RPN2 knockdown cell line. HSP70 promoter-driven cypridina luciferase activity (HSP70-CLuc) was normalized to the thymidine kinase promoter-driven gaussia luciferase activity (TK-GLuc). MM231-LN shNC or MM231-LN shRPN2 cells were transfected with 200 ng of pHSP70-Cluc in combination with 200 ng of pTK-Gluc. Transfection and luciferase assays were performed as described in experimental procedure. (d) HSF1 restored the HSP70 expression in MM231-LN shRPN2 cells. MM231-LN shRPN2 cells were transfected with pFlag-HSF1 with 200 ng of pHSP70-Cluc, or pSV40-Cluc in combination with 100 ng of pTK-Gluc, and luciferase activity was measured at 48 h after transfection. (e) GSK3β inhibitor restored HSF1 transcriptional activity. Six hours after transfection, cells were exposed to CHIR99021 (3, 10 μM) or an equivalent volume of dimethyl sulfoxide as a control added to the growth medium (CHIR99021, 0 μM). Treatments lasted for 72 h, after which the luciferase activity was examined. (f) Rescue experiment using MM231-LN shRPN2-UTR cells. RPN2-MF restored the HSP70 activity in MM231-LN shRPN2-UTR cells. pHSP70-Cluc was transfected into MM231-LN shRPN2-UTR cells with 300 ng of pCMV-RPN2-MF, or pEGFP-N1 in combination with 100 ng of pTK-Gluc, and luciferase activity was measured at 48 h after transfection. Full-length gels and blots are shown in supplementary figure 15.

ferase (HSP70-Cluc, Fig. 5c). Luciferase assays showed that RPN2 knockdown induced a 50% repression of HSF1 activity (Fig. 5c). When Flag-HSF1 was transfected with HSP70-Cluc in MM231-LN shRPN2 cells, luciferase activity was markedly enhanced 1.5- to 3-fold compared with those transfected with SV40 promoter-driven secreted cypridina luciferase (SV40-Cluc, Fig. 5d). We also confirmed that GSK3β inhibitor restored the HSF1 transcriptional activity in MM231-LN shRPN2 cells (Fig. 5e).

We also examined whether HSF1 activity correlated with RPN2 expression using MM231-LN cells expressing HSP70 promoter-driven GFP (MM231-LN HSP70-GFP) (Suppl. Fig. S5B). Flow cytometry and qRT-PCR analysis of MM231-LN HSP70-GFP cells showed that HSP70 and RPN2 were more highly expressed in the GFP high cell fraction than in the GFP low cell fraction (Suppl. Fig. S5C and 5D).

Finally, to exclude the off-target effects of shRNA against RPN2, we performed the rescue experiment using MM231-LN cells expressing shRNA against the 3′-untranslated region of RPN2 (Suppl. Fig.5E, MM231-LN shRPN2-UTR) to replace endogenous RPN2 with ectopically expressed RPN2-MF. Compared to the co-expression of shRPN2-UTR with GFP, co-expression of shRPN2-UTR with RPN2-MF restored the HSF1 activity in MM231-LN shRPN2-UTR cells (fig. 5f). These results strongly suggest that the formation of RPN2/GSK3β protein complexes inhibits the function of GSK3β, and that RPN2 knockdown induces the destabilization of mtp53 by GSK3β−mediated inactivation of heat shock proteins, leading to CSC phenotypic suppression.

RPN2 knockdown induces mtp53 degradation. Since RPN2 knockdown promoted GSK3β−mediated inactivation of heat shock proteins that are essential for mtp53 stabilization[6,25], we examined the expression and stability of mtp53 in MCF7-ADR and MM231-LN cells that express a p53 deletion mutant (p53 deletion 126–133)[34] and a p53 point mutant (p53R280K)[5], respectively (Fig. 6a and b). Immunoblot analysis with MCF7-ADR and MM231-LN cells showed that RPN2 knockdown induced mtp53 downregulation (Fig. 6b). As the lentivirus vector expressing shRPN2 also expressed the reporter gene GFP, mtp53 expression was examined in GFP-positive cells. Immunofluorescence staining with anti-p53 and anti-GFP antibodies revealed that mtp53 levels were considerably reduced in cells expressing shRPN2 compared with those expressing shNC (Fig. 6c). QRT-PCR revealed that *p53* mRNA levels were not altered in MM231-LN shRPN2 cells (Fig. 6d). Therefore, the protein stability of mtp53 was examined in RPN2 knockdown cells by cycloheximide (CHX) treatment (Fig. 6e). Immunoblot analysis showed that RPN2 knockdown reduced the half-life of mtp53 compared to the control (Fig. 6e and Suppl. Fig. S6). These findings were confirmed by RPN2 and mtp53 immunohistochemical staining in mouse MM231-LN tumors. Accumulation of mtp53 was observed in primary tumors with strong RPN2 expression but was reduced in primary tumors with low RPN2 expression (Fig. 6f). Immunohistochemical staining for RPN2 and mtp53 expression in breast cancer tissues yielded similar results to those obtained using tissues from subjects with a high incidence of lymph node metastasis (Fig. 6g and Suppl. Fig. S7).

To further elucidate the role of RPN2 in tumor initiation and metastasis, we performed label-free proteomic analysis, two-dimensional image-converted analysis of liquid chromatography and mass spectrometry (2DICAL)[35], and identified proteins differentially expressed between MM231-LN shRPN2 and MM231-LN shNC cells (Fig. 7a–c and Suppl. Table S1). Although several proteins were differentially expressed, we focused on 14-3-3zeta upregulation, which has been implicated in breast cancer pathogenesis[36,37]. Despite the suppression of CSC phenotypes by RPN2 knockdown (Fig. 1–6), 14-3-3zeta was upregulated in RPN2 knockdown cells, which is a typical feature of the early stages of breast cancer wherein 14-3-3zeta upregulation promotes wtp53 degradation via phosphorylation of the MDM2 E3 ligase, and thus, cancer progression[36,37]. Although the peptide specificity was very low, 2DICAL also showed that RPN2 knockdown induced the downregulation of mtp53 (Suppl. Table S1). Consistent with previous reports[36,37], we confirmed that N-terminal Halo-tagged 14-3-3zeta (H-14-3-3zeta) induced downregulation of wtp53 in MCF7 cells (Fig. 7d). Determination of the effect of 14-3-3zeta upregulation on the mtp53 protein stability revealed that H-14-3-3zeta expression partially induced RPN2 expression in MM231-LN cells (Fig. 7e). We also observed that RPN2 overexpression induced mtp53 upregulation in MM231-LN cells (Fig. 7f) and that mtp53 knockdown strongly reduced the expression of 14-3-3zeta in MM231-LN cells (Fig. 7g). Moreover, 14-3-3zeta knockdown reduced the expression of RPN2 in MM231-LN cells (Fig. 7h and Suppl. Fig. S18). These results suggest that 14-3-3zeta-mediated RPN2 upregulation contributes to the stability and accumulation of mtp53 and that RPN2 knockdown inhibits the 14-3-3zeta-dependent feedback regulation of mtp53 protein stability (Suppl. Fig S8).

Discussion

LOF or mtp53 accumulation is associated with acquisition of the EMT phenotype and development of high-grade tumors in breast cancers[11]. The half-life of wtp53 is < 30 min, whereas mtp53 is more stable, with a half-life of several hours[34,38]. Although the molecular mechanism of mtp53 stabilization is not completely understood, recent studies demonstrated that the contribution of mtp53 to tumor progression and its promotion of EMT onset account for the development of CSC properties[11,14]. Several pathways such as Wnt/β-catenin, TGF-β, Notch and Hedgehog signaling are critical for the acquisition of CSC properties[20]. In the present study, we provide evidence that the expression of RPN2 is regulated by p53 mutant (R280K and del126-133) which is associated with the acquisition of EMT phenotype in breast cancer and that RPN2 regulates CSC phenotypes via stabilization of mtp53 (R280K and del126-133). We demonstrated that shRNA-mediated knockdown of RPN2 significantly suppresses the CSC phenotype *in vitro* and *in vivo* and promotes GSK3β-mediated destabilization of mtp53.

While GSK3β promotes ubiquitin-proteasome pathway-mediated β-catenin degradation[39] and suppresses Snail expression at transcriptional and post-transcriptional levels[15,16], it is unclear how GSK3β suppresses CSC tumorigenesis and metastasis. Our results demonstrate, for the first time, a novel role for GSK3β in mtp53 destabilization and indicate that its activity is regulated by RPN2 (Fig. 4–6). We also demonstrated that RPN2 antagonized GSK3β function via physical interaction, and identified N-terminal amino acids 56–85 of GSK3β as important for its interaction with RPN2 (Fig. 4). Our previous study showed that RPN2 affects docetaxel resistance by modulating the *N*-linked glycosylation of P-glycoprotein[19]. Ribophorin-1 (RPN1) is also a component of the oligosaccharide transferase (OST) complex[40,41]. However, a recent study showed that RPN1 regulates the cell surface localization of μ-opioid receptor (MOR) via direct interaction with MOR[42]. Therefore, our data suggest that, in addition to being a component of the OST complex, RPN2 may play an important role in tumor onset and metastasis.

HSP90 is a promising therapeutic target for cancer therapy because the HSP90 chaperone machinery is upregulated and activated in malignant cancers and inhibition of this single protein causes the simultaneous degradation of multiple oncoproteins[8,9]. The stabilization and accumulation of mtp53 is associated with the formation of stable protein complexes between HSP90 and various types of mtp53, and the formation of such complexes inhibits the constitutive E3 ligase activity of MDM2 and CHIP[6,25]. Therefore, the identification and development of HSP90 inhibitors has been a focus of several studies[8,43]. One of main problems associated with the inhibition of HSP90 is the HSF1-dependent induction of HSP70

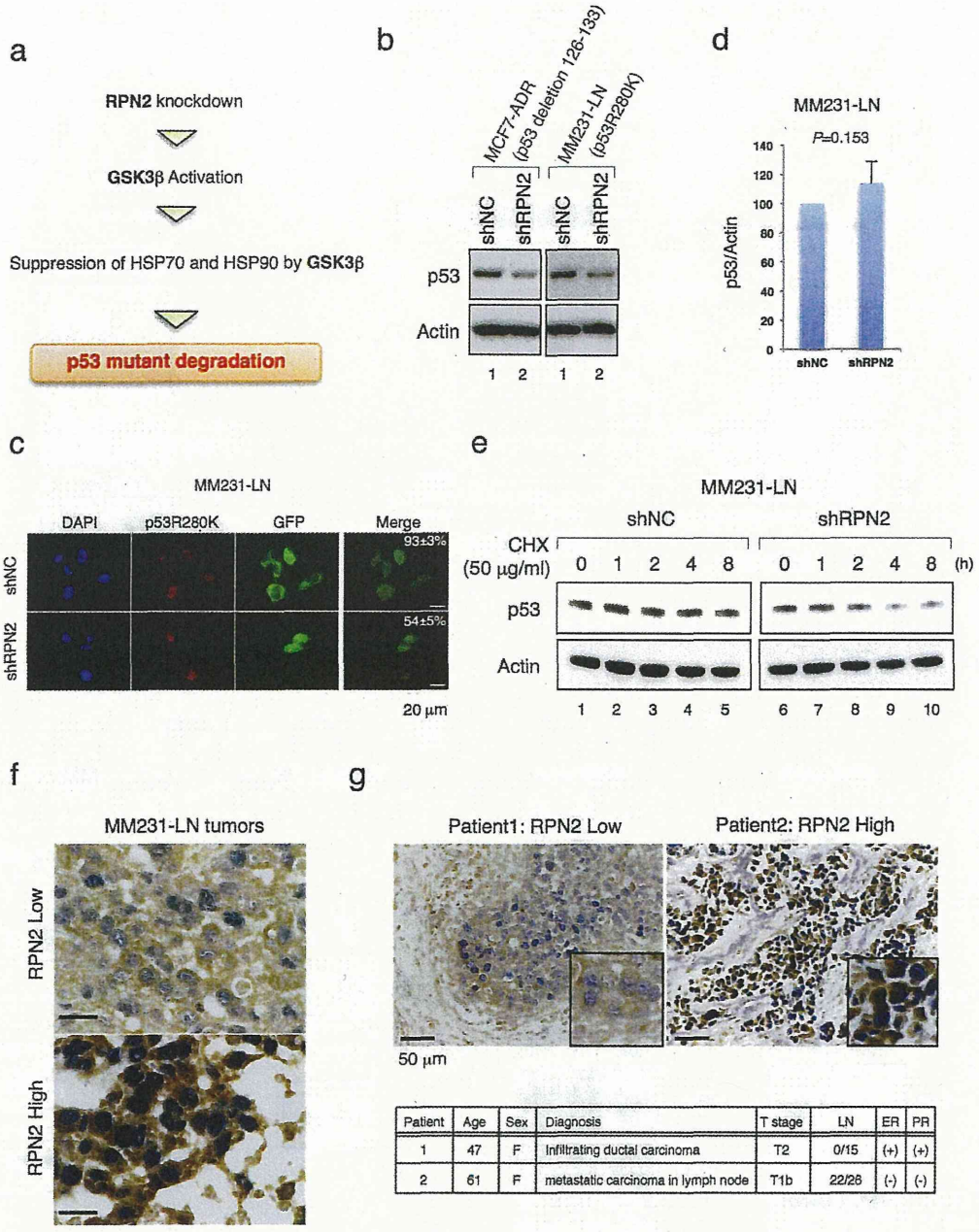

Patient	Age	Sex	Diagnosis	T stage	LN	ER	PR
1	47	F	Infiltrating ductal carcinoma	T2	0/15	(+)	(+)
2	61	F	metastatic carcinoma in lymph node	T1b	22/26	(-)	(-)

Figure 6 | RPN2 knockdown induces mtp53 degradation. (a) Working model for GSK3β-mediated downregulation of mtp53 in RPN2 knockdown cells. (b) and (d) Expression of mutant p53 (mtp53) in MCF7-ADR and MM231-LN cells. (c) Expression of mtp53 in MM231-LN shNC and MM231-LN shRPN2 cells. Immunofluorescence staining of mtp53 (Red) and GFP (Green) and merged images are shown. Nuclei are shown in blue (DAPI). Scale bar, 20 μm. (e) RPN2 knockdown reduced mtp53 protein stability. MM231-LN shNC and MM231-LN shRPN2 cells were treated with cycloheximide (50 μg/ml) for 0–8 h. Cell lysates were subjected to western blotting with anti-p53 and anti-actin antibodies. (f) Expression of RPN2 and mtp53 in MM231-LN tumors in mice. Panels show representative immunohistochemistry results for RPN2 (Brown) and mtp53 (Blue) in MM231-LN tumors. Scale bar, 20 μm. (g) The status of RPN2 (Brown) and mtp53 (Blue) in breast cancer tissues. The tissue sections obtained from patients were classified by the extent of lymph node metastasis (LN). ER, Estrogen Receptor; PR, Progesterone Receptor. Scale bar, 50 μm. Full-length gels and blots are shown in supplementary figure 16.

and HSP27 in response to HSP90 inhibitor treatment[8,9]. Considering that HSP70 chaperones also act as co-chaperones for HSP90 and have a well-documented antiapoptotic function that is independent of their interaction with HSP90[9,44], our finding that RPN2 knockdown suppresses HSP70 expression (Fig. 6) is important not only for understanding the regulation of mtp53 stability, but also for developing ways to overcome the side effects of HSP90 inhibitors.

We also found that 14-3-3zeta involved in the stabilization and accumulation of mtp53 (Fig. 7 and Suppl. Fig S8). Since forced expression of 14-3-3zeta showed only a modest effect on RPN2 expression in MM231-LN (Fig. 7e), it might be necessary to consider the other molecules and pathways that regulate RPN2 expression. In a clinical study, the upregulation of *14-3-3zeta* via amplification of the chromosome region where it is located (8q22) promoted chemoresistance to anthracyclines and metastatic recurrence of breast

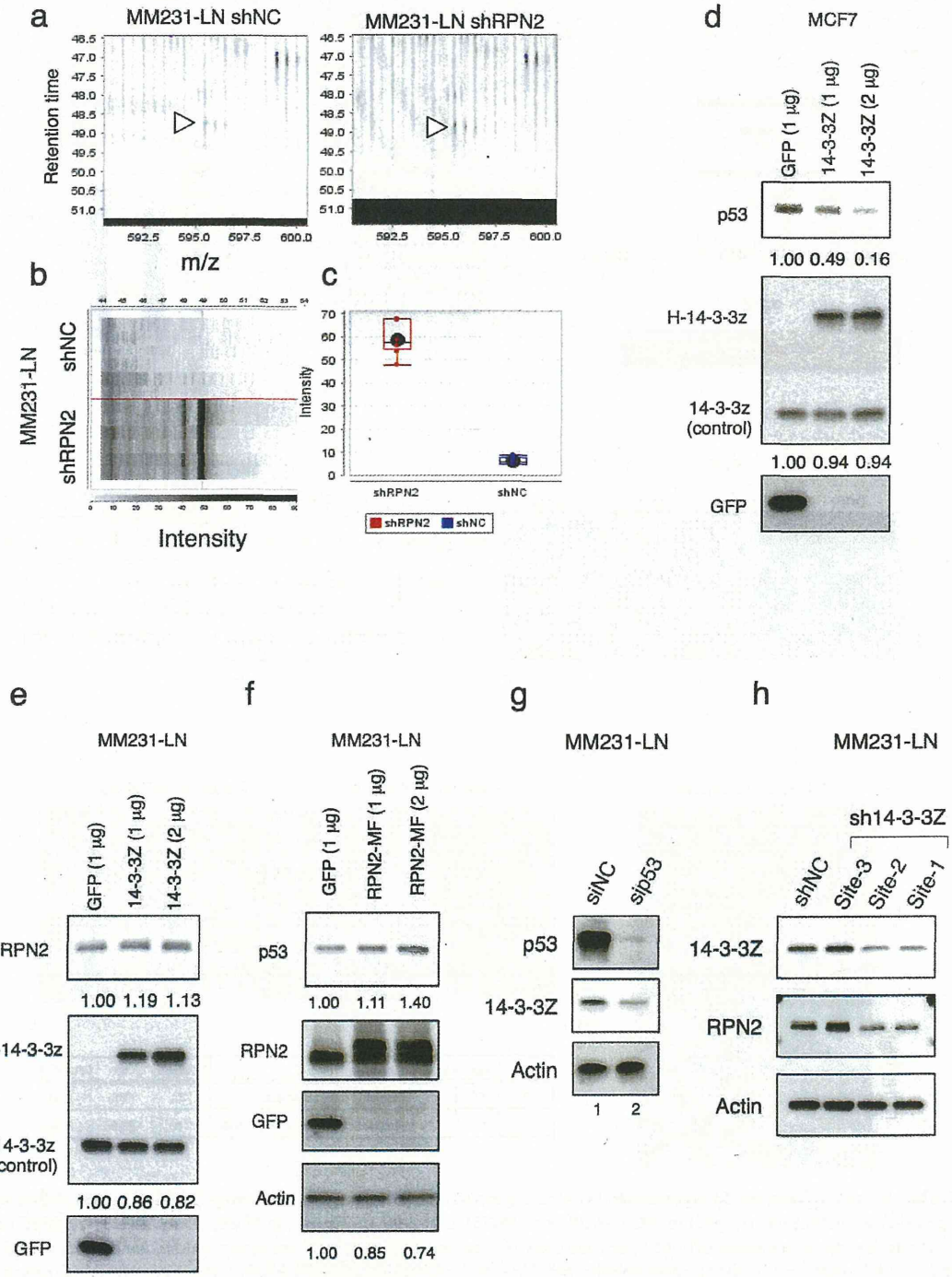

Figure 7 | 14-3-3zeta-mediated RPN2 upregulation is required for the mtp53 stability. (a) Detected peptides that differed between RPN2 knockdown cell line (MM231-LN shRPN2) and control (MM231-LN shNC). MS peak of 14-3-3Zeta (1433Z) in MM231-LN shNC (Right) and MM231-LN shRPN2 (Left) (indicated by arrows). (b) Gel-like views of MS peaks with retention time (RT) along the vertical axes (top) and distribution of the mean peak intensity of duplicates (bottom) across 6 samples. (c) Spot intensity of 14-3-3Z in MM231-LN shNC and MM231-LN shRPN2. (d) 14-3-3zeta reduced wtp53 expression. Lysates from MCF7 cells, transfected as indicated, were immunoblotted as shown. (e) and (f) RPN2 stabilized mtp53 in MM231-LN cells. Lysates from MM231-LN cells, transfected as indicated, were immunoblotted as shown. (g) and (h) 14-3-3zeta-dependent feedback regulation of mtp53 protein stability. Full-length gels and blots are shown in supplementary figure 17 and 18.

cancer[45]. However, the molecular mechanism underlying the chemoresistance and tumor recurrence has not been addressed. A recent study also showed that anthracyclines increase the amount of mtp53 mRNA and protein[46]. Therefore, the present study provides further insight into these mechanisms by showing that 14-3-3zeta promotes breast cancer malignancy.

TP53 mutations are present in 80% of triple-negative breast cancers (TNBC), which are characterized by the lack of estrogen and

progesterone receptors and the absence of human epidermal growth factor receptor 2[47]. Patients with TNBC show resistance to conventional chemotherapies and are in need of effective therapeutic agents to prevent recurrence and improve survival[48]. As shown in Figures 6g and S7, high expression of RPN2 and accumulation of mtp53 were observed in clinical samples of breast cancer tissues associated with lymph node metastasis. Moreover, our results are supported by a recent clinical study that showed that HSP70 expression correlates significantly with metastasis in TNBC patients[49]. Therefore, the concomitant expression of RPN2 and mtp53 could be a novel diagnostic marker for malignant progression and poor prognosis in TNBC. This is currently being investigated in a large cohort of TNBC patients at our NCC hospital and it would reveal that which types of p53 mutants are associated with RPN2 expression.

In summary, the present results indicate that inhibition of the RPN2/mtp53 regulatory network is a promising approach for overcoming the progression of malignant breast tumors and suppressing the CSC phenotype. Furthermore, our data suggest a novel mechanism for the modulation of nucleocytoplasmic proteins in cancer biology. Given the diverse biological roles of RPN2, further investigation aimed at understanding the role of RPN2 in processes associated with tumor progression is warranted.

Methods

Plasmids. N-terminal Flag-tagged Snail (pFlag-Snail), N-terminal Flag-tagged HSF1 (pFlag-HSF1), pBabe-puro-Snail, C-terminal V5-tagged wtp53 (pLenti6/V5-p53), C-terminal V5-tagged mtp53 (R280K, pLenti6/V5-p53R280K) and C-terminal HA-tagged GSK3β (pcDNA3-GSK3β-HA) were purchased from Addgene. To obtain C-terminal Myc- and Flag-tagged RPN2 constructs (pLenti-RPN2-Myc-Flag), cDNA encoding full-length human RPN2 (GenBank accession number Y00282) was amplified by polymerase chain reaction (PCR) using cDNA pools from MDA-MB231-D3H2-LN cells (MM231-LN). PCR fragments were inserted into EcoRI- and NotI-treated pLenti-C-Myc-DDK (Origene: PS100064). To obtain a HSP70 promoter-driven GFP (pHSP70-GFP), HSP70 promoter region was amplified by PCR using genomic DNA from MM231-LN cells (GenBank accession number M11717). The PCR fragment was inserted into BglII- and SalI-treated pEGFP-1 (Clontech). To obtain a HSP70 promoter-driven secreted cypridina luciferase (pHSP70-CLuc), HSP70-GFP was digested with KpnI and NotI and the fragment containing GFP was replaced with cypridina luciferase gene derived from pCLuc-Basic2 (NEB). All constructs were verified by DNA sequencing.

Cell culture. MCF7, MCF7-ADR, MCF7-ADR-Luc, MM231-LN, 293T, MCF10A and HME cells have been described previously[14,19]. To establish MM231-LN cells expressing HSP70-GFP, pHSP70-GFP containing the neomycin resistance gene was transfected with lipofectamine LTX (Invitrogen). The transfected cells were cultivated under selective growth medium including G418 (0.6 mg/ml). For spheroid culture, cells were plated on NanoCulture plates (Scivax) and cultured for 3 days.

Antibodies. The primary antibodies and dilutions were anti-RPN2 (1 : 2000, sc-166421, Santa Cruz Biotechnology), anti-p53 (1 : 2000, sc-126, Santa Cruz Biotechnology), anti-V5 (1 : 1000, V8137, Sigma), anti-Vimentin (1 : 2000, 550513, BD Pharmingen), anti-HA (1 : 2000, #3724, CST), anti-HSP27(1 : 2000, #2402, CST), anti-Myc (1 : 1000, 2278, CST), anti-Flag (1 : 1000, M185-7, MBL), anti-HA agarose (#3956S, CST), anti-HSP70 (1 : 1000, 610607, BD Transduction Laboratories), anti-HSP90 (1 : 1000, 610418, BD Transduction Laboratories), anti-GSK3β (1 : 1000, 610201, BD Transduction Laboratories), anti-Phospho-GSK3β (Tyr216) (1 : 1000, 612312, BD Transduction Laboratories), anti-N-cadherin (1 : 2000, #4061S, CST) and anti-actin antibodies (1 : 5000, MAB1501, Millipore). An anti-p53 antibody (Abcam, Pab240) was used for the detection of mtp53 by IHC. Staining was visualized using Alexa 488 or Alexa 594 (Molecular Probes). Immunofluorescence-stained cells were observed by fluorescence microscopy or confocal fluorescence microscopy (Leica). The signal intensity in immunoblot analysis was quantified using ImageJ software (http://rsbweb.nih.gov/ij/).

Lentiviral shRNA transduction. Cell lines stably expressing *RPN2* shRNA, *14-3-3zeta* shRNA or control non-target shRNA were established using a vector-based shRNA technique. Human *RPN2* shRNA targets 5′-GGAGGAGATTGAGGACCT TGT-3′ (shRPN2-site1), 5′-GCCACTTTGAAGAACCCAATC-3′ (shRPN2-site2), 5′-TCCAGATTGTAGTTATACTTC-3′ (shRPN2-UTR), human *14-3-3zeta* shRNA targets 5′-GCAGAGAGCAAAGTCTTCTAT-3′ (sh14-3-3zeta-site1), 5′-GCAAT TACTGAGAGACAACTT-3′ (sh14-3-3zeta-site2), 5′-GCTCGAGAATACAGAG AGAAA-3′ (sh14-3-3zeta-site3), 5′-GAGAGGAATCTTCTCTCAGTT-3′ (sh14-3-3zeta-site4), 5′-CTCTGTGTTCTATTATGAGAT-3′ (sh14-3-3zeta-site5) and control shRNA targets 5′-GAAATGTACTGCGCGTGGAGAC-3′. Briefly, each fragment was subcloned into pGreenPuro (System Biosciences). Recombinant lentiviruses were produced according to the manufacturer's instructions. In knockdown experiments, MCF7-ADR and MM231-LN cells were infected with recombinant lentiviruses expressing control shRNA (shNC) or shRNA against RPN2 (shRPN2).

Matrigel invasion assay. The matrigel invasion assay was performed using the Matrigel Invasion Chamber (BD Bioscience) according to the manufacturer's protocol. In brief, 5×10^4 cells were plated in the upper chamber in serum-free media. The bottom chamber contained RPMI media with 10% FBS. After 24–48 h, the bottom of the chamber insert was fixed and stained with Diff-Quick stain. Cells on the stained membrane were counted under a dissecting microscope. Each membrane was divided into four quadrants and an average from all four quadrants was calculated. The matrigel invasion assays were performed with biological triplicates.

Dual luciferase assay. MM231-LN shNC or MM231-LNshRPN2 cells (2×10^4 cells) were seeded in a 24-well plate and cotransfected with HSF1 expression vector (pFlag-HSF1) in combination with reporter constructs of HSP70 promoter (pHSP70-Cluc), and SV40 promoter (pSV40-Cluc) using Lipofectamine 2000 (Invitrogen). The amount of plasmid DNA used in each experiment is indicated in the figure legends. A thymidine kinase promoter-driven secreted gaussia luciferase (pTK-Gluc, NEB) was mixed in a DNA–liposome complex as an internal control. Luciferase activity was quantified by a dual-luciferase assay system (NEB) and relative transactivation was calculated according to the manufacturer's instructions. All experiments were repeated at least 3 times.

Fluorescence-activated cell sorting. FITC or APC-conjugated anti-CD44 antibody (BD Bioscience, clone G44-26), PE-conjugated anti-CD24 antibody (Biolegend, clone LM5), APC-conjugated anti-E cadherin antibody (Biolegend, clone 67A4) and propidium iodide (5 μg/ml) were used for fluorescence-activated cell sorting (FACS) analysis using JSAN in accordance with the manufacturer's protocols. Data were processed by FlowJo software.

Immunoprecipitation. MM231-LN cells were lysed using immunoprecipitation buffer (20 mM Tris–HCl pH 8.0, 150 mM NaCl, 1 mM EDTA, 0.1% NP-40, 10% glycerol, 1 mM DTT, protease inhibitor cocktail, phosphatase inhibitor). After brief sonication, the lysates were cleared by centrifugation at 4°C. Supernatants were incubated with anti-RPN2 or anti- anti-GSK3β antibodies for 4 h and protein A/G-Sepharose beads (Invitrogen) for 4 h at 4°C. The immunocomplexes were washed four times, boiled in sample buffer and immunoblotted with anti-GSK3β, anti-Phospho-GSK3β (Tyr216) and anti-RPN2 antibodies.

Co-immunoprecipitation analysis. Extracts of 293T cells were obtained using immunoprecipitation buffer as described above. Supernatants were incubated with anti-HA Agarose (CST) under rotation for 4 h at 4°C. After washing four times with immunoprecipitation buffer, the immunoprecipitated protein complex bound to the beads was eluted with the HA peptide (Wako). The eluates from the immunoprecipitation and cell lysates were immunoblotted with anti-GSK3β, anti-Phospho-GSK3β (Tyr216) and anti-GFP antibodies.

Real-time reverse transcription PCR. Total RNA was isolated from cells and tumor tissues with an RNeasy Mini Kit and an RNase-Free DNase Set (Qiagen), and cDNA was produced with an ExScript RT reagent Kit (Takara). The cDNA samples were subjected to real-time PCR with SYBR Premix Ex Taq (Invitrogen) and specific primers (Supplementary Methods). All reactions were performed in a Light Cycler (Applied Biosystems). Gene expression levels were normalized to those of β-actin.

Bioluminescence imaging. Animal experiments were performed in compliance with the guidelines of the Institute for Laboratory Animal Research, National Cancer Center Research Institute. Female non-obese diabetic/severe combined immunodeficiency (NOD/SCID) mice (NOD.CB17-Prdkc^{scid}/J, CLEA Japan, Shizuoka, Japan) aged 4–6 weeks were anaesthetized by exposure to 3% isoflurane on day zero and subsequent days. Images were analyzed with Living Image software (Xenogen, part of Caliper Life Sciences). Bioluminescent flux (photonss^{-1} sr^{-1} cm^{-2}) was determined for the primary tumors, lungs or lymph nodes (upper abdomen, region of interest).

Mammary fat pad xenografts. MCF7-ADR or MM231-LN cells were suspended in a PBS/Matrigel (Sigma) mixture (1 : 1) and injected into the mammary fat pad in a 50 μl volume (n = 5 each and 10^2–10^6 cells per animal).

Tissue arrays. The tissue arrays of breast cancer samples were purchased from Super Bio CHIP. Immunohistochemical staining of RPN2 and mutant p53 was performed with DAB peroxidase and alkaline phosphatase substrate kits (Vector Laboratories).

Statistical analysis. Data are presented as mean ± standard error of the mean (s.e.m.) or mean ± standard deviation (s.d.). Statistical significance was determined by Student's two-tailed *t*-test unless otherwise noted. A P value < 0.05 was considered statistically significant.

1. Shaulian, E., Zauberman, A., Ginsberg, D. & Oren, M. Identification of a minimal transforming domain of p53: negative dominance through abrogation of sequence-specific DNA binding. *Mol Cell Biol* **12**, 5581–5592 (1992).
2. Kalo, E. *et al.* Mutant p53 attenuates the SMAD-dependent transforming growth factor beta1 (TGF-beta1) signaling pathway by repressing the expression of TGF-beta receptor type II. *Mol Cell Biol* **27**, 8228–8242 (2007).
3. Muller, P. A. *et al.* Mutant p53 drives invasion by promoting integrin recycling. *Cell* **139**, 1327–1341 (2009).
4. Song, H., Hollstein, M. & Xu, Y. p53 gain-of-function cancer mutants induce genetic instability by inactivating ATM. *Nat Cell Biol* **9**, 573–580 (2007).
5. Adorno, M. *et al.* A Mutant-p53/Smad complex opposes p63 to empower TGFbeta-induced metastasis. *Cell* **137**, 87–98 (2009).
6. Li, D., Marchenko, N. D. & Moll, U. M. SAHA shows preferential cytotoxicity in mutant p53 cancer cells by destabilizing mutant p53 through inhibition of the HDAC6-Hsp90 chaperone axis. *Cell Death Differ* **18**, 1904–1913 (2011).
7. Peng, Y., Chen, L., Li, C., Lu, W. & Chen, J. Inhibition of MDM2 by hsp90 contributes to mutant p53 stabilization. *J Biol Chem* **276**, 40583–40590 (2001).
8. Trepel, J., Mollapour, M., Giaccone, G. & Neckers, L. Targeting the dynamic HSP90 complex in cancer. *Nat Rev Cancer* **10**, 537–549 (2010).
9. Powers, M. V., Clarke, P. A. & Workman, P. Dual targeting of HSC70 and HSP72 inhibits HSP90 function and induces tumor-specific apoptosis. *Cancer Cell* **14**, 250–262 (2008).
10. Yan, W. *et al.* Histone deacetylase inhibitors suppress mutant p53 transcription via histone deacetylase 8. *Oncogene* (2012).
11. Chang, C. J. *et al.* p53 regulates epithelial-mesenchymal transition and stem cell properties through modulating miRNAs. *Nat Cell Biol* **13**, 317–32 (2011).
12. Onder, T. T. *et al.* Loss of E-cadherin promotes metastasis via multiple downstream transcriptional pathways. *Cancer Res* **68**, 3645–3654 (2008).
13. Oft, M., Akhurst, R. J. & Balmain, A. Metastasis is driven by sequential elevation of H-ras and Smad2 levels. *Nat Cell Biol* **4**, 487–494 (2002).
14. Mani, S. A. *et al.* The epithelial-mesenchymal transition generates cells with properties of stem cells. *Cell* **133**, 704–715 (2008).
15. Bachelder, R. E., Yoon, S. O., Franci, C., de Herreros, A. G. & Mercurio, A. M. Glycogen synthase kinase-3 is an endogenous inhibitor of Snail transcription: implications for the epithelial-mesenchymal transition. *J Cell Biol* **168**, 29–33 (2005).
16. Yook, J. I. *et al.* A Wnt-Axin2-GSK3beta cascade regulates Snail1 activity in breast cancer cells. *Nat Cell Biol* **8**, 1398–1406 (2006).
17. Li, Y. *et al.* Sulforaphane, a dietary component of broccoli/broccoli sprouts, inhibits breast cancer stem cells. *Clin Cancer Res* **16**, 2580–2590 (2010).
18. Gupta, P. B. *et al.* Identification of selective inhibitors of cancer stem cells by high-throughput screening. *Cell* **138**, 645–659 (2009).
19. Honma, K. *et al.* RPN2 gene confers docetaxel resistance in breast cancer. *Nat Med* **14**, 939–948 (2008).
20. Clevers, H. The cancer stem cell: premises, promises and challenges. *Nat Med* **17**, 313–319 (2011).
21. Yin, H. & Glass, J. The phenotypic radiation resistance of CD44+/CD24(-or low) breast cancer cells is mediated through the enhanced activation of ATM signaling. *PloS one* **6**, e24080 (2011).
22. Calcagno, A. M. *et al.* Prolonged drug selection of breast cancer cells and enrichment of cancer stem cell characteristics. *Journal of the National Cancer Institute* **102**, 1637–1652 (2010).
23. Al-Hajj, M., Wicha, M. S., Benito-Hernandez, A., Morrison, S. J. & Clarke, M. F. Prospective identification of tumorigenic breast cancer cells. *Proc Natl Acad Sci U S A* **100**, 3983–3988 (2003).
24. Todaro, M. *et al.* Colon cancer stem cells dictate tumor growth and resist cell death by production of interleukin-4. *Cell Stem Cell* **1**, 389–402 (2007).
25. Li, D. *et al.* Functional inactivation of endogenous MDM2 and CHIP by HSP90 causes aberrant stabilization of mutant p53 in human cancer cells. *Mol Cancer Res* **9**, 577–588 (2011).
26. Muller, P., Hrstka, R., Coomber, D., Lane, D. P. & Vojtesek, B. Chaperone-dependent stabilization and degradation of p53 mutants. *Oncogene* **27**, 3371–3383 (2008).
27. Esser, C., Scheffner, M. & Hohfeld, J. The chaperone-associated ubiquitin ligase CHIP is able to target p53 for proteasomal degradation. *J Biol Chem* **280**, 27443–27448 (2005).
28. Zhang, Y. *et al.* HSF1-dependent upregulation of Hsp70 by sulfhydryl-reactive inducers of the KEAP1/NRF2/ARE pathway. *Chem Biol* **18**, 1355–1361 (2011).
29. Chiang, W. C., Ching, T. T., Lee, H. C., Mousigian, C. & Hsu, A. L. HSF-1 regulators DDL-1/2 link insulin-like signaling to heat-shock responses and modulation of longevity. *Cell* **148**, 322–334 (2012).
30. Xavier, I. J. *et al.* Glycogen synthase kinase 3beta negatively regulates both DNA-binding and transcriptional activities of heat shock factor 1. *J Biol Chem* **275**, 29147–29152 (2000).
31. Kim, D., Kim, S. H. & Li, G. C. Proteasome inhibitors MG132 and lactacystin hyperphosphorylate HSF1 and induce hsp70 and hsp27 expression. *Biochem Biophys Res Commun* **254**, 264–268 (1999).
32. Liu, J. *et al.* p27 suppresses arsenite-induced Hsp27/Hsp70 expression through inhibiting JNK2/c-Jun- and HSF-1-dependent pathways. *J Biol Chem* **285**, 26058–26065 (2010).
33. Wei, L. *et al.* Hsp27 participates in the maintenance of breast cancer stem cells through regulation of epithelial-mesenchymal transition and nuclear factor-kappaB. *Breast Cancer Res* **13** (2011).
34. Ogretmen, B. & Safa, A. R. Expression of the mutated p53 tumor suppressor protein and its molecular and biochemical characterization in multidrug resistant MCF-7/Adr human breast cancer cells. *Oncogene* **14**, 499–506 (1997).
35. Ono, M. *et al.* Prolyl 4-hydroxylation of alpha-fibrinogen: a novel protein modification revealed by plasma proteomics. *J Biol Chem* **284**, 29041–29049 (2009).
36. Neal, C. L. & Yu, D. 14-3-3zeta as a prognostic marker and therapeutic target for cancer. *Expert Opin Ther Targets* **14**, 1343–1354 (2010).
37. Danes, C. G. *et al.* 14-3-3 zeta down-regulates p53 in mammary epithelial cells and confers luminal filling. *Cancer Res* **68**, 1760–1767 (2008).
38. Zambetti, G. P. & Levine, A. J. A comparison of the biological activities of wild-type and mutant p53. *FASEB J* **7**, 855–865 (1993).
39. Cohen, P. & Frame, S. The renaissance of GSK3. *Nat Rev Mol Cell Biol* **2**, 769–776 (2001).
40. Crimaudo, C., Hortsch, M., Gausepohl, H. & Meyer, D. I. Human ribophorins I and II: the primary structure and membrane topology of two highly conserved rough endoplasmic reticulum-specific glycoproteins. *EMBO J* **6**, 75–82 (1987).
41. Wilson, C. M., Roebuck, Q. & High, S. Ribophorin I regulates substrate delivery to the oligosaccharyltransferase core. *Proc Natl Acad Sci U S A* **105**, 9534–9539 (2008).
42. Ge, X., Loh, H. H. & Law, P. Y. mu-Opioid receptor cell surface expression is regulated by its direct interaction with Ribophorin I. *Mol Pharmacol* **75**, 1307–1316 (2009).
43. Mehta, P. P. *et al.* Effective targeting of triple-negative breast cancer cells by PF-4942847, a novel oral inhibitor of Hsp 90. *Clin Cancer Res* **17**, 5432–5442 (2011).
44. Yiu, C. C. *et al.* Down-regulation of heat-shock protein 70 (HSP-70) correlated with responsiveness to neoadjuvant aromatase inhibitor therapy in breast cancer patients. *Anticancer Res* **30**, 3465–3472 (2010).
45. Li, Y. *et al.* Amplification of LAPTM4B and YWHAZ contributes to chemotherapy resistance and recurrence of breast cancer. *Nat Med* **16**, 214–218 (2010).
46. Bug, M. & Dobbelstein, M. Anthracyclines induce the accumulation of mutant p53 through E2F1-dependent and -independent mechanisms. *Oncogene* (2011).
47. Cleator, S., Heller, W. & Coombes, R. C. Triple-negative breast cancer: therapeutic options. *Lancet Oncol* **8**, 235–244 (2007).
48. Gluz, O. *et al.* Triple-negative breast cancer--current status and future directions. *Ann Oncol* **20**, 1913–1927 (2009).
49. Sun, B. *et al.* Identification of metastasis-related proteins and their clinical relevance to triple-negative human breast cancer. *Clin Cancer Res* **14**, 7050–7059 (2008).

Acknowledgments

We thank Dr S. Koizumi for providing the human mammary carcinoma cell lines MCF7, MCF7-ADR and MDA-MB-231-D3H2-LN, Dr Y. Yamamoto for helpful discussions and Miss. A. Inoue for her excellent technical assistance. This study was supported in part by a grant-in-aid for the Third-Term Comprehensive 10-Year Strategy for Cancer Control of Japan, a grant-in-aid for Scientific Research on Priority Areas Cancer from the Japanese Ministry of Education, Culture, Sports, Science and Technology, and the Program for Promotion of Fundamental Studies in Health Sciences of the National Institute of Biomedical Innovation of Japan, and supported by a Funding Program for World-Leading Innovative R&D on Science and Technology (FIRST Program) from the Japan Society for the Promotion of Science (JSPS).

Author contributions

R.T. and K.H. designed the experiments and analysed the data. R.T. and F.T. performed the experiments. K.K. provided human breast cancer pathology information. M.O. performed proteome analysis by 2DICAL. R.T. and T.O. wrote the manuscript. All authors discussed the results and commented on the manuscript.

Additional information

Supplementary information accompanies this paper at http://www.nature.com/scientificreports

Competing financial interests: The authors declare no competing financial interests.

How to cite this article: Takahashi, R.-u. *et al.* Ribophorin-2 regulates breast tumor initiation and metastasis through the functional suppression of GSK3β. *Sci. Rep.* 3, 2474; DOI:10.1038/srep02474 (2013).

⌘ *Author's Choice*

THE JOURNAL OF BIOLOGICAL CHEMISTRY VOL. 288, NO. 15, pp. 10849–10859, April 12, 2013

Neutral Sphingomyelinase 2 (nSMase2)-dependent Exosomal Transfer of Angiogenic MicroRNAs Regulate Cancer Cell Metastasis*[S]

Received for publication, December 18, 2012, and in revised form, February 18, 2013 Published, JBC Papers in Press, February 25, 2013, DOI 10.1074/jbc.M112.446831

Nobuyoshi Kosaka[‡], Haruhisa Iguchi[‡§], Keitaro Hagiwara[‡¶], Yusuke Yoshioka[‡1], Fumitaka Takeshita[‡], and Takahiro Ochiya[‡2]

From the [‡]Division of Molecular and Cellular Medicine, National Cancer Center Research Institute, 5-1-1, Tsukiji, Chuo-ku, Tokyo 104-0045, Japan, the [§]Pharmacology Research Laboratories, Dainippon Sumitomo Pharma Co., Ltd., 1-98 Kasugadenaka 3-chome, Konohana-ku, Osaka 554-0022, Japan, and the [¶]Department of Biological Information, Graduate School of Bioscience and Biotechnology, Tokyo Institute of Technology, Yokohama, Kanagawa 226-8501, Japan

Background: Contribution of exosomal microRNAs to cancer metastasis remains unknown.
Results: Exosomal angiogenic microRNAs secreted by metastatic cancer cells promote the metastasis through the activation of endothelial cells.
Conclusion: Horizontal transfer of exosomal miRNAs from cancer cells can dictate the microenviromental niche for the benefit of the cancer cell.
Significance: This is the first to connect cancer metastasis to the exosomal microRNA *in vivo*.

The release of humoral factors between cancer cells and the microenvironmental cells is critical for metastasis; however, the roles of secreted miRNAs in non-cell autonomous cancer progression against microenvironmental cells remain largely unknown. Here, we demonstrate that the neutral sphyngomyelinase 2 (nSMase2) regulates exosomal microRNA (miRNA) secretion and promotes angiogenesis within the tumor microenvironment as well as metastasis. We demonstrate a requirement for nSMase2-mediated cancer cell exosomal miRNAs in the regulation of metastasis through the induction of angiogenesis in inoculated tumors. In addition, miR-210, released by metastatic cancer cells, was shown to transport to endothelial cells and suppress the expression of specific target genes, which resulted in enhanced angiogenesis. These findings suggest that the horizontal transfer of exosomal miRNAs from cancer cells can dictate the microenviromental niche for the benefit of the cancer cell, like "on demand system" for cancer cells.

The secretion of humoral factors from cancer cells to microenvironmental cells is essential for metastasis during cancer development (1). Although microRNAs (miRNAs)[3] are known as tumor suppressors of cell autonomous malignancy phenotypes such as metastasis (2) and multidrug resistancy (3), the roles of miRNAs in non-cell autonomous cancer progression against microenvironmental cells remain largely unknown. The existence of secretory RNA has been known for many years (4, 5), and recent reports have shown that miRNAs (6), which regulate various types of biological phenomena through the regulation of a variety of target genes, are secreted from cells via the exosome (7, 8). These findings have raised the possibility that RNAs, including miRNAs, may serve as novel humoral factors in cell-cell communication (9). We recently demonstrated that miRNAs are released through neutral sphingomyelinase 2 (nSMase2)-regulated secretory machinery and that these secretory miRNAs are transferable and functional in recipient cells (10). Furthermore, we also found that a tumor-suppressive miRNA secreted from non-cancerous cells via this pathway could be transported between cells and exert gene silencing in the recipient cancer cells, thereby leading to an inhibition of cancer cell growth (11). In the last few years, it has become clear that exosomal miRNAs play critical roles in mediating cell-cell communication, specifically between immune cells, endothelial cells and cancer cells (12–17). These findings provide evidence that exosomal miRNAs are required for cell-cell communication in various physiological and pathological conditions, although the contribution of extracellular miRNAs to cancer metastasis remains largely unknown (9). Here, we first demonstrated that horizontal transfer of exosomal miR-210 from metastatic cancer cells could dictate the microenvironmental endothelial cells to the benefit of the cancer cells, which contributed to cancer metastasis. Preventing the expression of

* This work was supported in part by a grant-in-aid for the third term comprehensive 10-year strategy for cancer control, a grant-in-aid for scientific research on priority areas cancer from the Ministry of Education, Culture, Sports, Science, and Technology, and the Program for Promotion of Fundamental Studies in Health Sciences of the National Institute of Biomedical Innovation (NiBio), and the Japan Society for the Promotion of Science through the Funding Program for world leading innovative R&D on science and technology (FIRST Program) initiated by the Council for Science and Technology Policy, and a grant-in-aid for Scientific Research on Innovative Areas (functional machinery for non-coding RNAs) from the Japanese Ministry of Education, Culture, Sports, Science, and Technology.
⌘ *Author's Choice*—Final version full access.
[S] This article contains supplemental Figs. 1–9.
[1] A research fellow for the Japan Society for the Promotion of Science.
[2] To whom correspondence should be addressed: Div. of Molecular and Cellular Medicine, National Cancer Center Research Inst., 1-1 Tsukiji, 5-chome, Chuo-ku, Tokyo 104-0045, Japan. Tel.: 81-3-3542-2511 (ext. 4800); Fax: 81-3-5565-0727; E-mail: tochiya@ncc.go.jp.

[3] The abbreviations used are: miRNA, microRNA; nSMase2, neutral sphingomyelinase 2; KD, knockdown; luc, luciferase; HUVEC, human umbilical cord vein endothelial cell; nSMase2-OE, nSMase2-overexpressing cancer cells; qRT-PCR, quantitative RT-PCR.

nSMase2 in metastatic cancer cells abrogates the metastatic ability of cancer cells to target lung tissues, whereas reconstitution via the administration of exosomes isolated from metastatic cancer cells rescued this phenomenon. In this context, the number of endothelial cells in inoculated tumors was proportional to the expression level of nSMase2 in cancer cells. In fact, exosomes derived from a metastatic cancer cell line enhanced the capillary formation and migration of endothelial cells *in vitro*. Interestingly, the expression profiles of exosomal miRNAs obtained from metastatic cancer cells demonstrated that a set of angiogenic miRNAs were highly concentrated in these exosomes. One of them, miR-210, enhanced the angiogenesis through the suppression of specific target gene, which resulted in enhanced angiogenesis. These results revealed that cancer cells provide nSMase2-regulated exosomal miRNAs to endothelial cells to promote their metastatic initiation efficiency.

EXPERIMENTAL PROCEDURES

Reagents—Goat polyclonal anti-Alix (Q-19; sc-49268) and donkey anti-goat IgG (HRP; sc-2020) were purchased from Santa Cruz Biotechnology. Mouse monoclonal anti-HSP70, clone 7/HSP70 (610607), and mouse monoclonal ant-human CD63 antibody (556019) were purchased from BD Biosciences. Rabbit polyclonal anti-CD31 antibody (ab28364) was from Abcam. Peroxidase-labeled anti-mouse antibodies were purchased from GE Healthcare (NA931V). GW4869 was purchased from Calbiochem (Darmstadt, Germany). Geneticin and puromycin were purchased from Invitrogen.

Cell Culture—4T1 cells, a mouse breast cancer cell line, MCF7, non-metastatic breast cancer cells, and MCF10A, normal mammary epithelial cells, were obtained from the American Type Culture Collection (Manassas, VA). MDA-MB-231-D3H1 and MDA-MB-231-D3H2LN, a metastatic human breast cancer cell line, were obtained from Xenogen. 4T1, MCF7, MDA-MB-231-D3H1, and MDA-MB-231-D3H2LN were cultured in RPMI containing 10% heat-inactivated FBS and antibiotic-antimycotic (Invitrogen) at 37 °C in 5% CO_2. Human umbilical cord vein endothelial cells (HUVECs) were purchased from Lonza and cultured in EBM-2 BulletKit (Lonza) supplemented with 2% FBS.

Exosome Purification—Exosomes were purified by differential centrifugation as described previously (10). The exosome fraction was measured for its protein content using the Micro BCA protein assay kit (Thermo Scientific, Wilmington, DE).

Tube Formation Assay—HUVECs (100,000) cells were cultured on 150 μl of Matrigel (Sigma) in culture medium for 16 h in 24-well plate. The degree of tube formation was quantified by measuring the number of branches in five randomly chosen fields from each well using NIH ImageJ software. For rescue experiments, HUVECs were transfected using Dharmafect reagent (Dharmacon) according to the manufacturer's recommendations with anti-control or anti-miR-210 (Ambion). After 24 h of posttransfection, cells were seeded onto Matrigel as described above with 1 μg of exosome.

Establishment of Stable Cell Lines—A stable 4T1 and MDA-MB-231-D3H2LN nSMase2-modified cell lines that expressed mouse nSMase2 shRNA, human nSMase2 shRNA, and pCT-CD63-GFP were generated by selection with puromycin. A stable 4T1 and MDA-MB-231-D3H2LN cell lines that overexpresses human nSMase2 were generated by selection with geneticin. 4T1 cells or MDA-MB-231-D3H2LN were transfected with 0.5 μg of the vector at 90% confluency in 24-well dishes using a Lipofectamine LTX reagent in accordance with the manufacturer's instructions.

Co-culture Experiments—Well inserts for 24-well plates with a 0.4-μm pore-sized filter were purchased from BD and used following the manufacturer's instructions. 4T1 control cells, 4T1-nSMase2-KD cells, 4T1-siLuc cells, or 4T1-CD63-GFP cells (100, 000) were seeded into the well inserts. HUVECs (200, 000) were seeded into 24-well plates.

Confocal Microscopy—Confocal microscopy was done on an Olympus laser scanning microscope FV10i (Olympus). Filters used were 489–510 nm (GFP and Alexa Fluor 488) and 577–603 nm (Alexa Fluor 568).

Immunoblot Analysis—Exosomes were lysed in a 2% SDS buffer, and equal amounts of protein were loaded onto an SDS-PAGE gel. Anti-Alix (1:200), anti-HSP70 (1:1,000), and anti-CD63 (1:200) were used as primary antibodies. The dilution ratio of each antibody is indicated in *parentheses*. Two secondary antibodies (peroxidase-labeled anti-goat and anti-mouse antibodies) were used at a dilution of 1:2000. Bound antibodies were visualized by chemiluminescence using the ImmunoStar LD (290-69904) (Wako), and luminescent images were analyzed by a LuminoImager (LAS-3000; Fujifilm, Inc.). Only gels for CD63 (BD Biosciences) detection were run under non-reducing conditions.

Plasmids—psiRNA-LucGL3 was purchased from InvivoGen. Knockdown shRNA vector for human and mouse nSMase2 were purchased from TaKaRa Bio. A full-length human nSMase2 cDNA was cloned into pIRES2-EGFP vector (Clontech). Primary miR-210 were PCR-amplified from human genomic DNA and cloned into the downstream of CMV promoter in pIREShyg3 (Takara Bio). The sensor vector for miR-210 was constructed by introducing tandem binding sites with perfect complementarity to miR-210, separated by a four-nucleotide spacer into the XhoI site of psiCHECK2 (Promega). The sequences of the binding site are as follows: 5′-TTCTCGAGTTTCAGCCG-CTGTCACACGCACAGTTACGCGTTTTCAGCCGCTGT-CACACGCACAGTTCTCGAGTT-3′ (sense) and 5′-AACTC-GAGAACTGTGCGTGTGACAGCGGCTGAAAACGCGT-AACTGTGCGTGTGACAGCGGCTGAAACTCGAGAA-3′ (antisense). The "seed" sequence of miR-210 is *underlined*. In a mutated miR-210 sensor vector, the seed sequence, ACACGCA, was displaced with TGTGCGT. All of the plasmids were verified by DNA sequencing.

Isolation of RNAs—Isolation of exosomal and cellular RNAs was performed using the miRNeasy Mini Kit (Qiagen). Exosome or cell lysate was diluted with 1 ml of Qiazol solution. Subsequent extraction and filter cartridge work were carried out according to the manufacturer's protocol.

mRNA and miRNA Expression Analysis—The method for qRT-PCR has been described previously (10). PCR was carried out in 96-well plates using the 7300 Real Time PCR system (Applied Biosystems). All reactions were done in triplicate. All TaqMan MicroRNA assays were purchased from Applied Bio-